ACS APPLIED MATERIALS & INTERFACES

Research Article

www.acsami.org

Seeding Atomic Layer Deposition of Alumina on Graphene with Yttria

Arjun Dahal,[†] Rafik Addou,[‡] Angelica Azcatl,[‡] Horacio Coy-Diaz,[†] Ning Lu,[‡] Xin Peng,[‡] Francis de Dios,[‡] Jiyoung Kim,[‡] Moon J. Kim,[‡] Robert M. Wallace,[‡] and Matthias Batzill*[,†]

[†]Department of Physics, University of South Florida, Tampa, Florida 33620, United States

[‡]Department of Materials Science and Engineering, University of Texas at Dallas, Richardson, Texas 75080, United States

ABSTRACT: Integrating graphene into nanoelectronic device structure requires interfacing graphene with high-κ dielectric materials. However, the dewetting and thermal instability of dielectric layers on top of graphene makes fabricating a pinhole-free, uniform, and conformal graphene/dielectric interface challenging. Here, we demonstrate that an ultrathin layer of high-κ dielectric material Y_2O_3 acts as an effective seeding layer for atomic layer deposition of Al_2O_3 on graphene. Whereas identical Al_2O_3 depositions lead to discontinuous film on bare graphene, the Y_2O_3 seeding layer yields uniform and conformal films. The morphology of the Al_2O_3 film is characterized by atomic force microscopy and transmission electron microscopy. C-1s X-ray photoemission spectroscopy indicates that the underlying graphene remains intact following Y_2O_3 seed and Al_2O_3 deposition. Finally, photoemission measurements of the graphene/SiO_2/Si, Y_2O_3/graphene/SiO_2, and Al_2O_3/Y_2O_3/graphene/SiO_2 interfaces indicate n-type doping of graphene with different doping levels due to charge transfer at the interfaces.

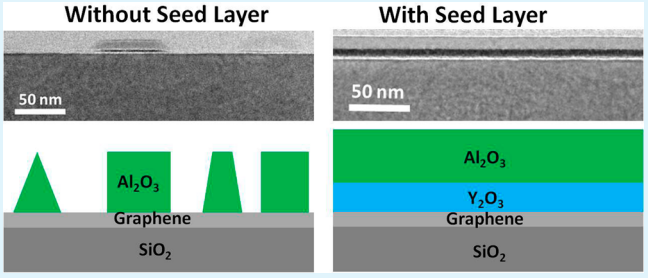

KEYWORDS: *graphene, dielectric, Al_2O_3, seed layer, Y_2O_3, doping, X-ray photoemission spectroscopy*

INTRODUCTION

Deposition of high quality high-κ dielectrics on graphene is required for isolating top-gates in graphene field-effect devices. For better performance of field-effect transistors (FETs), these dielectric thin films should be ultrathin, conformal, and pinhole-free with minimal disorder or traps at the dielectric−graphene interface. Atomic layer deposition (ALD) is a preferred technique for achieving high-quality, conformal, ultrathin dielectric films with precise thickness control while preventing physical damage to the interface by energetic particles. However, the low surface energy of graphene basal planes does not provide appropriate nucleation sites for the ALD precursors, whereas step edges of graphene are selectively decorated by ALD. To address this issue, either graphene has been modified (for example, by fluorine[1] or physisorbed ozone[2]) or seed layers (organic[3] or inorganic[4,5]) have been grown on top of graphene before the growth of metal-oxide dielectric materials. Surface modification of graphene may lead to degradation of its electronic properties due to damages in graphene,[6] whereas seed layers increase the thickness and reduce the effective κ value of the gate dielectric, resulting in an overall decrease in capacitance.[3]

Numerous high-κ dielectric materials, including alumina (Al_2O_3), have been investigated as potential dielectrics for graphene devices.[2−4,7] Several intrinsic properties of alumina make it the preferred candidate for the gate dielectric material in graphene FETs. First, the high dielectric constant of alumina (κ = 10) allows device operation at a higher electric field, taking advantage of the high breakdown field. Second, the large bandgap of alumina (E_g = 7 eV) relative to other high-κ dielectric materials enables adequate barrier heights at the interface. However, the deposition of high quality alumina on graphene remains a challenge.

We recently demonstrated that yttria (Y_2O_3) monolayers wet graphene supported on metal surfaces.[8] We also demonstrated that good quality, crystalline yttria films can be grown on top of metal-supported graphene.[9] Our finding of the good wetting behavior of yttria on sp^2 carbon is in agreement with previous reports for yttria growth on graphene or carbon nanotube device structures.[7,10,11] Although yttria is a high-κ dielectric in its own right, it exhibits only acceptable properties as a crystalline material. In most applications, amorphous dielectrics are preferred in order to obtain uniform properties and avoid lateral property variations due to difficulty in avoiding crystal defects.

In this paper, we investigate if the superior wetting behavior of yttria on graphene can be combined with the superior dielectric properties of (amorphous) alumina to make better dielectric layers. We demonstrate the use of ultrathin yttria layers for seeding the conformal growth of alumina by ALD. The potential advantage of yttria as seed layers over polymer seed layers is that yttira is a high-κ dielectric material and this

Received: November 20, 2014
Accepted: January 2, 2015
Published: January 2, 2015

DOI: 10.1021/am508154n
ACS Appl. Mater. Interfaces 2015, 7, 2082−2087

will not lead to a decrease in the capacitance of the gate dielectric layer. Also, formation of charge trap sites within the dielectric layer should be reduced in a pure-oxide dielectric. It is worth mentioning that in a related approach hexagonal boron nitride (h-BN) has been recently used as a buffer layer in deposition of alumina on graphene.[12] In that report, h-BN was mechanically transferred onto graphene, while our approach is a direct growth of yttria on graphene. The advantages of our growth process versus a transfer process are in the conformity of the grown films and easier scalability of growth processes.

In this study, we chose CVD-grown graphene transferred to SiO_2/Si as a convenient substrate for the study of dielectric deposition. We have previously shown that yttria deposition on metal supported graphene[8,9] as well as on graphene transferred to SiO_2[10] results in a uniform and pinhole-free film; this suggests that the graphene substrate material does not affect the wetting behavior of yttria on graphene significantly and thus the approach described here may be applicable to other supported graphene systems. As has been shown in the past, CVD-grown graphene can be successfully transferred to numerous flat substrates like SiO_2.[13−15] Furthermore, our group has also transferred CVD-grown graphene to $SrTiO_3$,[16] MoS_2,[17] and sulfur-protected W(110)[18] and in all of these studies we could show that a clean interface can be obtained by annealing in an ultrahigh vacuum (UHV). Here we show by atomic force microscopy (AFM), transmission electron microscopy (TEM), and low energy ion scattering spectroscopy (ISS) that the alumina film deposited on a yttria seed on the graphene/SiO_2 sample is uniform, pinhole-free, and conformal. Furthermore, X-ray photoemission spectroscopy (XPS) characterizations indicate that the graphene is n-type doped when it is supported on the SiO_2/Si substrate. Moreover, the n-type doping of graphene is increased by deposition of the low-work function yttria layer.

EXPERIMENTAL DETAIL

Graphene was prepared by chemical vapor deposition (CVD) growth in a tube furnace on high purity copper foil. Before transferring graphene to the SiO_2/Si substrates, graphene on copper foil was spin-coated with a layer of poly methyl methacrylate (PMMA) followed by chemical etching of the copper in ammonium persulfate. The graphene/PMMA was then rinsed in DI water and captured with a SiO_2/Si substrate. Subsequently, the PMMA covered graphene supported on SiO_2 substrate was first dried at room temperature (RT) and then annealed at 180 °C in air. At 180 °C, the PMMA melts and helps to make the graphene flat on the substrate. PMMA from the graphene was removed by dipping the sample in acetone for 3 h. To further remove any organic residues from the surface, the graphene covered SiO_2 sample was annealed in a tube furnace at 350 °C for 3 h.

Graphene/SiO_2 samples were loaded into a multichamber UHV system, described in detail elsewhere.[19] This system allows sample transfer in UHV to an analysis chamber for XPS and ISS characterization, to a physical vapor deposition (PVD) chamber for yttria deposition, and to an ALD reactor for alumina deposition. Graphene/SiO_2 samples were annealed in UHV at 300 °C for 3 h prior to yttria deposition. A thin yttria seed layer is deposited on top of the graphene/SiO_2 sample by reactive electron beam deposition of yttrium from a water-cooled electron beam evaporator in a 10^{-7} Torr oxygen atmosphere at RT. The complete oxidation and formation of Y_2O_3 was confirmed by in situ XPS. For another set of experiments on graphene/SiO_2 and highly ordered pyrolytic graphite (HOPG) samples, the yttria film was deposited in a separate UHV system (similar growth conditions as in the multichamber UHV system) and yttria growth was monitored by Auger electron spectroscopy (AES) (AES data are not presented). These samples were then transported through air and loaded into the multichamber UHV system for ALD growth of alumina and further XPS characterization. The results for the ex situ prepared yttria films were identical to those of in situ grown yttria, suggesting that the yttria is quite stable under environmental exposure. Alumina was deposited on the yttria covered graphene/SiO_2 sample in a Picosun SUNALE ALD reactor at 300 °C using trimethylaluminum (TMA) and water precursors. A single ALD cycle corresponds to the following precursor exposure sequence: TMA 0.1s → N_2 4s → H_2O 0.1s → N_2 4s. Graphene/SiO_2, yttria/graphene/SiO_2, and alumina/yttria/graphene/SiO_2 samples were characterized in situ by XPS and ISS and ex situ by AFM and TEM. The thickness of the alumina and yttria films on the graphene/SiO_2 samples were measured by TEM. For some samples, the thicknesses of the alumina and yttria films were estimated by comparing the time of deposition (keeping all the deposition conditions the same) with TEM-calibration measurements.

XPS spectra were collected using a monochromatic Al Kα X-ray ($h\nu$ = 1486.7 eV) source and Omicron EA125 hemispherical analyzer. All the spectra were measured at 45° emission with a 15 eV analyzer pass energy. The C-1s core level was modeled by fitting it with a Doniach−Sunjic peak shape to accommodate for the typical asymmetric line shape of sp^2 carbon. The graphene sp^2 components of the post-transfer C-1s spectra were fitted with a full width at half-maximum (fwhm) of 0.71 eV, based on previously reported results produced on the same XPS system for the C-1s spectrum of graphene on Cu prior to transfer.[15] Potential charging of the sample during XPS measurements was compensated for by keeping the Si-2p core level peak fixed to the value before any oxide deposition.

In ISS, the kinetic energy of the scattered He^+ ions was detected with the same energy analyzer as that for XPS with reversed voltages. The primary energy of the He^+ ions was 1000 eV, and the scattering angle between a fine focused ion gun and the detector was 37°. A typical spectrum was acquired in 5 min. Due to a small fluorine contamination in the ALD system, we always observe a minor F-peak in the ISS spectrum.

RESULTS AND DISCUSSION

Prior to alumina deposition, we have performed ex situ characterization of the seed layer morphology by AFM. Figure 1a shows an AFM image recorded on ∼1.5 nm yttria film deposited on a graphene/SiO_2 sample. The morphology of the yttria film is uniform, and there is no indication of cluster formation. The good wetting behavior of yttria is not particular to graphene but is universal for sp^2 carbon.[9] To illustrate good wetting behavior of yttria for all sp^2 carbon, we also deposited ∼1.5 nm of yttria film on HOPG. It is important to note that the HOPG sample should be thoroughly outgassed prior to yttria growth; otherwise, nonuniform yttria films are obtained. Parts b−d of Figure 1 show AFM images measured on the room temperature deposited yttria film on HOPG samples outgassed in UHV at 400, 500, and 700 °C, respectively. It is apparent that the surface morphology of the yttria film deposited on HOPG outgassed at 700 °C is very smooth. In comparison, the yttria films deposited on HOPG outgassed at low temperatures (400 and 500 °C) exhibit clustering and a tendency to decorate step edges of HOPG. For other high-κ dielectric materials such as alumina and hafnium oxide (HfO_2) deposited on bare graphene or graphite, patchy and discontinuous surface morphologies have been reported.[20] Thus, our results for yttria indicate quite favorable growth on sp^2 carbon. Although the reason behind the much better wetting behavior of yttria compared to other traditional high-κ dielectric materials is not understood, it is worth mentioning that yttria is not a unique metal oxide in terms of wetting sp^2 carbon. For instance, recent reports show that europium oxide growth on graphite also exhibits a wetting of the graphite surface.[21]

DOI: 10.1021/am508154n
ACS Appl. Mater. Interfaces 2015, 7, 2082−2087

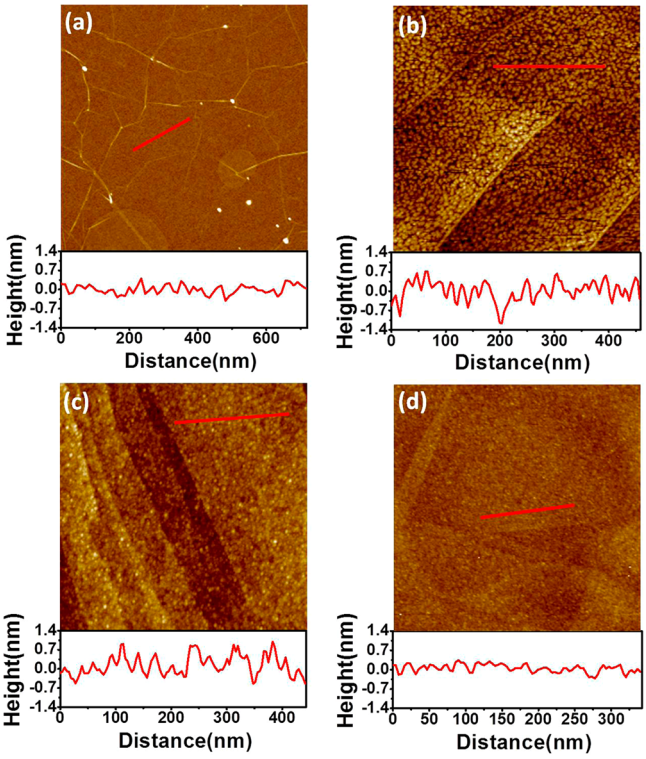

Figure 1. AFM images and line scans of yttria films on graphene and HOPG. (a) AFM image (3 μm × 3 μm) of ~1.5 nm of yttria film on graphene/SiO_2. AFM images (1 μm × 1 μm) of ~1.5 nm of yttria film deposited on HOPG outgassed at 400, 500, and 700 °C are shown in parts b, c, and d, respectively. The yttria was deposited at room temperature for all the samples.

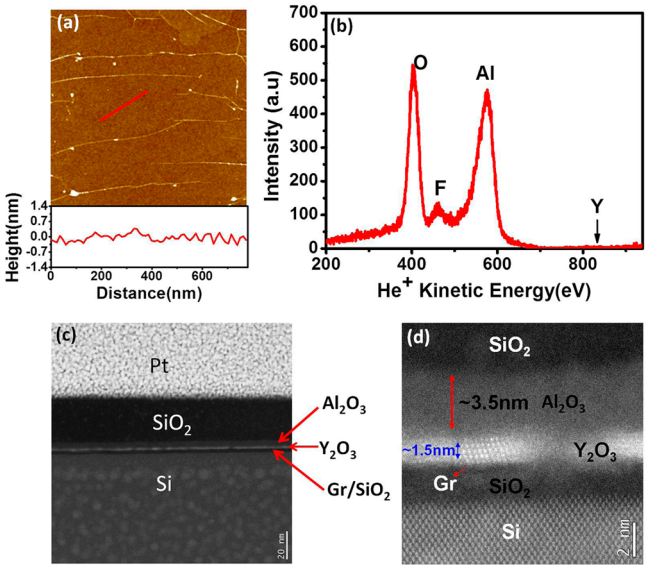

Figure 2. AFM, ISS, and TEM measurements acquired on ~3.5 nm of alumina film on graphene/SiO_2 with yttria as a seed layer. (a) AFM image (3 μm × 3 μm) with line scan of alumina film on yttria/graphene/SiO_2. The alumina film is uniform and conformal. (b) ISS of the alumina film in part a. The absence of the Y peak in ISS shows that the alumina fully covers the yttria film. In ISS, a very small fluorine peak is observed due to contamination from the Viton seal in the ALD reactor. (c) Large scale scanning TEM image of the alumina/yttria/graphene/SiO_2 sample in part a. (d) Scanning TEM high angle annular dark field (HAADF) image of the alumina/yttria/graphene/SiO_2 sample. The yttria film is crystalline, while the alumina is amorphous. The graphene layer cannot be resolved in the TEM images.

Yttria covered graphene/SiO_2 samples were subsequently used as substrates for the growth of alumina by ALD. Figure 2a shows an AFM image measured after depositing 50 cycles (~3.5 nm) of alumina. The root-mean-square (rms) roughness of selected areas (excluding graphene wrinkles) of this sample is 0.24 nm, which is comparable to the rms roughness of 0.20 and 0.30 nm of the graphene/SiO_2 sample (Figure 3a) and the Y_2O_3/graphene/SiO_2 sample (Figure 1a), respectively. With the yttria seeding layer, the resulting alumina film is uniform and conformal. Without the yttria seed layer, the alumina film on graphene is nonuniform and nonconformal (discussed later). The alumina/yttria/graphene/SiO_2 sample was also characterized in situ by ISS. This technique is sensitive to only the topmost layer of the sample. Figure 2b shows ISS for 3.5 nm alumina film deposited on the yttria covered graphene/SiO_2 sample. The complete suppression of yttrium signal indicates that alumina fully covers the yttria film.

The alumina/yttria/graphene/SiO_2 sample was also characterized by TEM. Parts c and d of Figure 2 show large scale and high resolution scanning TEM (STEM) high angle annular dark filed (HAADF) images of the alumina/yttria/graphene/SiO_2 sample. The uniform thickness of the yttria plus alumina film in the TEM images suggests that the dielectric layer is uniform and likely pinhole-free. A uniform-thickness dielectric film is also in agreement with the lateral characterization by AFM. The STEM also suggests that the alumina film is amorphous while some crystalline grains are seen for the yttria seed layer. In addition to crystalline and noncrystalline areas in the yttria layer, Figure 2d also shows regions in which the contrast in STEM appears less bright, suggesting a lower density of yttrium. Since yttria and alumina form several strong mixed line phases, namely, $Y_3Al_5O_{12}$ (YAG) or $YAlO_3$ (YAP), we speculate that the alumina may react with yttria in regions where the yttria film had a high density of crystalline defects or was amorphous, which could facilitate a solid state reaction with the deposited alumina even at the low deposition temperatures.

In order to unambiguously demonstrate the seeding effect of yttria for the growth of uniform alumina films, we compared the growth of alumina on bare and yttria-covered graphene/SiO_2. For this, we covered half of the graphene/SiO_2 sample with a Ta-foil mask during the yttria growth. After yttria film deposition on graphene/SiO_2, the sample was taken out from the UHV, the shadow mask was removed, and the sample was characterized by AFM. Figure 3a shows the AFM image of the bare graphene on the SiO_2 substrate, and Figure 3e shows the other half of the sample that was covered with an ~5 nm yttria film. Comparison of parts a and e of Figure 3 indicates the uniformity of the yttria layer. After AFM characterization, the sample was reloaded into a UHV system and the sample was outgassed in UHV at 300 °C for 2 h before alumina deposition. Then, 100 cycles of alumina were deposited on the entire sample. Figure 3b shows the morphology of the alumina deposited on the bare graphene region. The rms roughness of the sample (excluding big clusters and graphene wrinkles) is 4.4 nm, which is much bigger than that of the alumina film with a seeding layer. The alumina film is nonconformal and discontinuous, which confirms previous reports of alumina deposition on nonfunctionalized graphene or graphite surfaces.[20] Parts c and d of Figure 3 show the large scale and high resolution TEM images of the alumina/graphene/SiO_2 region of the sample, respectively. The TEM images show that

DOI: 10.1021/am508154n
ACS Appl. Mater. Interfaces 2015, 7, 2082−2087

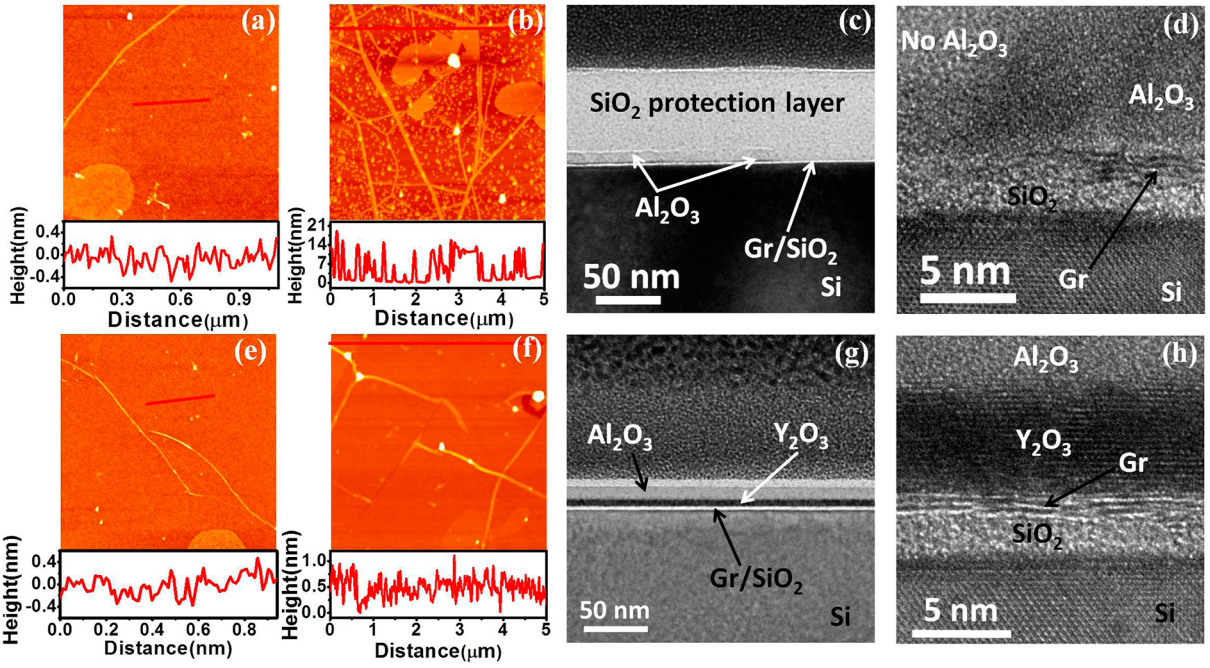

Figure 3. AFM and TEM images of alumina and yttria films. Half of the graphene/SiO_2 sample was shadow masked with Ta-foil during yttria deposition. Alumina film was deposited on the entire sample after removing the shadow mask. (a) AFM image (3 μm × 3 μm) with line scan of graphene on SiO_2/Si. (b) AFM image with line scan of 100 cycles of alumina film deposited on bare graphene/SiO_2. (c) Large scale and (d) high resolution TEM images of the alumina/graphene/SiO_2 region of the sample. Alumina film is missing in some area of the sample, indicating alumina film is not uniform on bare graphene. (e) AFM image (3 μm × 3 μm) with line scan of yttria film on graphene/SiO_2. (f) AFM image with line scan of 100 cycles of alumina film on top of yttria film. (g) Large scale and (h) high resolution TEM images of yttria film. The yttria film is uniform, pinhole-free, and crystalline. The alumina film on top of yttria film is also uniform and pinhole-free.

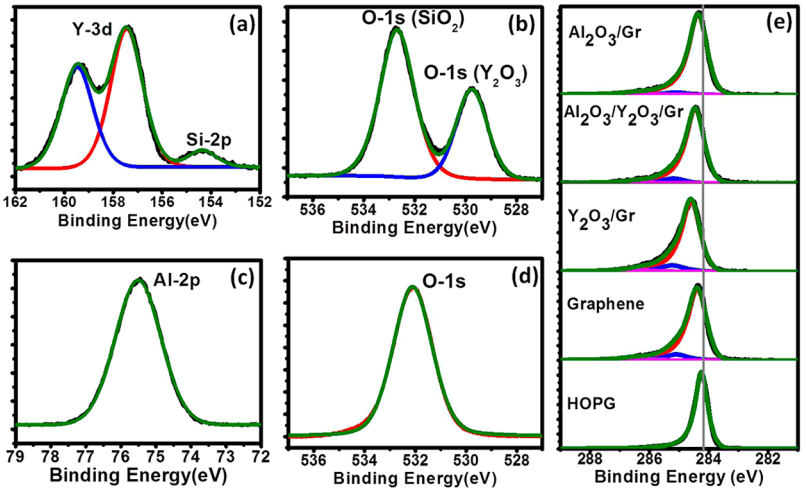

Figure 4. XPS measurements of HOPG and graphene samples. (a) Y-3d peak of the ~1.5 nm of yttria film deposited on the graphene sample. The Y-$3d_{5/2}$ peak is observed at 157.45 eV. (b) O-1s peak for the yttria/graphene/SiO_2 sample. The O-1s peak at 529.75 eV corresponds to yttria, and the peak at 532.7 eV corresponds to SiO_2. (c) Al-2p peak of ~3.5 nm of alumina film deposited on the yttria/graphene/SiO_2 sample. The Al-2p peak is observed at 75.5 eV. (d) O-1s peak of ~3.5 nm of alumina film. The O-1s peak is observed at 532.10 eV. (e) C-1s peaks for HOPG, graphene/SiO_2, yttria/graphene/SiO_2, alumina/yttria/graphene/SiO_2, and alumina/graphene/SiO_2 samples. The C-1s peak for HOPG is observed at 284.25 eV. For the graphene/SiO_2 sample, the C-1s core level is deconvoluted with a graphene component at 284.40 eV (red line) and two much smaller components at 285.1 ± 0.1 eV (blue line) and 286.5 ± 0.1 eV (pink line), which are attributed to carbon contamination and/or PMMA residue. The C-1s core levels are measured at 284.61, 284.46, and 284.37 eV for the yttria/graphene/SiO_2, alumina/yttria/graphene/SiO_2, and alumina/graphene/SiO_2 samples, respectively. For C-1s measurements, only 10 cycles of alumina are deposited on the yttria/graphene/SiO_2 and graphene/SiO_2 samples.

alumina is not covering large areas of the sample. In contrast, Figure 3f shows the AFM morphology of the alumina film deposited on the yttria precovered graphene. The alumina film is continuous and uniform. Parts g and h of Figure 3 show the large scale and high resolution TEM images of the alumina/yttria/graphene/SiO_2 region of the sample. TEM images show that the alumina film deposited on top of the yttria film is uniform and conformal.

To verify the chemical identity of the yttria and alumina films, XPS was performed on the in situ grown yttria/

DOI: 10.1021/am508154n
ACS Appl. Mater. Interfaces 2015, 7, 2082−2087

graphene/SiO_2 and alumina/yttria/graphene/SiO_2 samples. For the yttria/graphene/SiO_2 sample, the Y-3$d_{5/2}$ peak is observed at 157.45 eV and two components are observed for O-1s: the peak at 529.75 eV corresponds to Y_2O_3, and the peak at 532.7 eV corresponds to SiO_2. The Y-3d and O-1s peaks are shown in parts a and b of Figure 4, respectively. The binding energy difference between the O-1s peak in yttria and the Y-3d peak is measured to be 372.3 eV, which is consistent with a previous report for yttria.[22] For the alumina/yttria/graphene/SiO_2 sample, the Al-2p and O-1s peaks are shown in parts c and d of Figure 4, respectively. Furthermore, the Y-3d peak position does not change after alumina deposition (not shown). For thicker alumina films (~3.5 nm), XPS spectra show the Al-2p peak at 75.5 eV and a single O-1s peak at 532.10 eV. The binding energy difference between the O-1s and Al-2p peaks of 456.6 eV is consistent with previous reports for alumina.[23,24]

When graphene is in contact with another material, even in the absence of chemical bonding, charges are expected to be transferred across the interface in order to align the Fermi levels in the different materials. This results in charge doping of graphene and causes a shift of the C-1s core level of graphene in XPS measurements.[25] This shift of the C-1s core level is a consequence of the low density of states close to the Dirac point of graphene which causes a measurable shift of the Fermi level even for small interface charge transfers. Consequently, since in XPS the Fermi level is the reference energy level for core level binding energy, a shifting of the Fermi level causes an equal shift in the C-1s core level binding energy. For the Fermi level shift to be equal in magnitude to the C-1s core level shift, a rigid band model for graphene is assumed; i.e., the energy difference between the C-1s core level and the Dirac point is assumed to be unaffected by charge doping of graphene. In our experiments, we set this energy difference to the C-1s binding energy measured in HOPG. Thus, a shift of the C-1s core level in graphene relative to the C-1s core level in HOPG is interpreted as an equivalent shift of the Fermi level relative to the Dirac point in graphene.

For the graphene/SiO_2 sample, the C-1s core level was deconvoluted with a graphene component at 284.40 eV and two much smaller components at 285.1 ± 0.1 and 286.5 ± 0.1 eV, which are attributed to carbon contamination and/or PMMA residue.[15,26] The C-1s binding energies for the yttria/graphene/SiO_2, alumina/yttria/graphene/SiO_2, and alumina/graphene/SiO_2 samples were also deconvoluted in the same way as that for the graphene/SiO_2 sample. The C-1s core levels for HOPG, graphene/SiO_2, yttria/graphene/SiO_2, alumina/yttria/graphene/SiO_2, and alumina/graphene/SiO_2 are shown in Figure 4e. The C-1s binding energy of the graphene component for all the samples is compared to the binding energy of the HOPG sample measured in the same experimental setup. The C-1s core levels for the HOPG, yttria/graphene/SiO_2, alumina/yttria/graphene/SiO_2, and alumina/graphene/SiO_2 samples are measured to be 284.25, 284.61, 284.46, and 284.37 eV, respectively. As the alumina forms clusters on bare graphene, both bare graphene regions and alumina-covered regions contribute to the C-1s core level for the alumina/graphene/SiO_2 sample. However, no broadening of the C-1s peak after alumina deposition compared to the bare graphene/SiO_2 sample is detected, suggesting that the alumina does not induce a significant peak shift for the C-1s peak. For the alumina/yttria/graphene/SiO_2 and alumina/graphene/SiO_2 samples, C-1s measurements were taken for 10 cycles of alumina deposition on the yttria/graphene/SiO_2 and graphene/SiO_2 samples, respectively.

In all cases, we measure a larger C-1s binding energy for the graphene samples compared to HOPG. Assuming no chemical bonding between the oxides and graphene, this shift in the C-1s peak suggest a Fermi level shift above the Dirac point, i.e., n-type doping of the graphene. For bare graphene on SiO_2/p-type Si, we observe a ~0.15 eV shift of the Fermi level compared to charge neutral graphene. Alumina deposition on bare graphene (i.e., without a yttria seed layer) reduces this shift very slightly to ~0.12 eV; i.e., the graphene may be slightly less n-type doped after alumina deposition. On the other hand, deposition of yttria, a material with a well documented extremely small work function (the low work function makes yttria coating, e.g., useful for thermionic electron emitting filaments), increases the n-type doping to ~0.36 eV above the Fermi level, while additional deposition of alumina reduces the doping somewhat to ~0.21 eV. All of these shifts in the Fermi level of graphene are following trends in agreement with the work function differences of the materials; however, precise values are difficult to estimate because the work functions of dielectric materials are ill-defined. The fact that the charge doping in graphene is reduced after deposition of alumina also suggests that some effective work function for the yttria/alumina sandwich should be used. Finally, the fact that the low-work-function material yttria causes strong n-type doping in graphene may have some influence in the use of yttria seed layers for high-κ dielectrics in field effect devices, since the dielectric induced doping may have to be compensated for by the gate voltage.

CONCLUSION

We have demonstrated the utility of yttria as a seeding layer for ALD Al_2O_3 growth on graphene. The morphology of alumina film was characterized by AFM, ISS, and (S)TEM. It has been shown that the alumina film grown on a yttria seed layer is uniform, pinhole-free, and conformal. Formation of a yttria/alumina stack of dielectrics is expected to reduce the overall capacitance of the dielectric layer; however, this trade-off is currently needed for the growth of alumina based dielectrics on graphene. XPS measurements enabled the characterization of the interface charge transfer. The low work function of yttria is responsible for a strong n-type doping of graphene when interfaced with yttria. This doping is somewhat reduced after alumina deposition.

AUTHOR INFORMATION

Corresponding Author

*E-mail: mbatzill@usf.edu.

Notes

The authors declare no competing financial interest.

ACKNOWLEDGMENTS

This work was supported in part by the Southwest Academy on Nanoelectronics (SWAN) sponsored by the Nanoelectronic Research Initiative and by the Center for Low Energy Systems Technology (LEAST), one of six centers of STARnet, a Semiconductor Research Corporation program sponsored by MARCO and DARPA. The USF group acknowledges financial support from the National Science Foundation (NSF) under Award No. DMR-1204924.

DOI: 10.1021/am508154n
ACS Appl. Mater. Interfaces 2015, 7, 2082−2087

REFERENCES

(1) Robinson, J. T.; Burgess, J. S.; Junkermeier, C. E.; Badescu, S. C.; Reinecke, T. L.; Perkins, F. K.; Zalalutdniov, M. K.; Baldwin, J. W.; Culbertson, J. C.; Sheehan, P. E.; Snow, E. S. Properties of Fluorinated Graphene Films. *Nano Lett.* **2010**, *10*, 3001−3005.

(2) Jandhyala, S.; Mordi, G.; Lee, B.; Lee, G.; Floresca, C.; Cha, P.-R.; Ahn, J.; Wallace, R. M.; Chabal, Y. J.; Kim, M. J.; Colombo, L.; Cho, K.; Kim, J. Atomic Layer Deposition of Dielectrics on Graphene Using Reversibly Physisorbed Ozone. *ACS Nano* **2012**, *6*, 2722−2730.

(3) Alaboson, J. M. P.; Wang, Q. H.; Emery, J. D.; Lipson, A. L.; Bedzyk, M. J.; Elam, J. W.; Pellin, M. J.; Hersam, M. C. Seeding Atomic Layer Deposition of High-k Dielectrics on Epitaxial Graphene with Organic Self-Assembled Monolayers. *ACS Nano* **2011**, *5*, 5223−5232.

(4) Fallahazad, B.; Lee, K.; Lian, G.; Kim, S.; Corbet, C. M.; Ferrer, D. A.; Colombo, L.; Tutuc, E. Scaling of Al_2O_3 Dielectric for Graphene Field-Effect Transistors. *Appl. Phys. Lett.* **2012**, *100*, 093112.

(5) Han, W.; McCreary, K. M.; Pi, K.; Wang, W. H.; Li, Y.; Wen, H.; Chen, J. R.; Kawakami, R. K. Spin Transport and Relaxation in Graphene. *J. Magn. Magn. Mater.* **2012**, *324*, 369−381.

(6) Robinson, J. A.; LaBella, M.; Trumbull, K. A.; Weng, X.; Cavelero, R.; Daniels, T.; Hughes, Z.; Hollander, M.; Fanton, M.; Snyder, D. Epitaxial Graphene Materials Integration: Effects of Dielectric Overlayers on Structural and Electronic Properties. *ACS Nano* **2010**, *4*, 2667−2672.

(7) Kanayama, K.; Nagashio, K.; Nishimura, T.; Toriumi, A. Large Fermi Energy Modulation in Graphene Transistors with High-Pressure O_2-Annealed Y_2O_3 Topgate Insulators. *Appl. Phys. Lett.* **2014**, *104*, 083519.

(8) Addou, R.; Dahal, A.; Batzill, M. Growth of a Two-Dimensional Dielectric Monolayer on Quasi-Freestanding Graphene. *Nat. Nanotechnol.* **2013**, *8*, 41−45.

(9) Dahal, A.; Coy-Diaz, H.; Addou, R.; Lallo, J.; Sutter, E.; Batzill, M. Preparation and Characterization of Ni(111)/Graphene/Y_2O_3(111) Heterostructures. *J. Appl. Phys.* **2013**, *113*, 194305.

(10) Wang, Z.; Xu, H.; Zhang, Z.; Wang, S.; Ding, L.; Zeng, Q.; Yang, L.; Pei, T.; Liang, X.; Gao, M.; Peng, L. Growth and Performance of Yttrium Oxide as an Ideal High-κ Gate Dielectric for Carbon-Based Electronics. *Nano Lett.* **2010**, *10*, 2024−2030.

(11) Xu, H. L.; Zhang, Z. Y.; Xu, H. T.; Wang, Z. X.; Wang, S.; Peng, L. M. Top-Gated Graphene Field-Effect Transistors with High Normalized Transconductance and Designable Dirac Point Voltage. *ACS Nano* **2011**, *5*, 5031−5037.

(12) Han, Q.; Yan, B.; Gao, T.; Meng, J.; Zhang, Y.; Liu, Z.; Wu, X.; Yu, D. Boron Nitride Film as a Buffer Layer in Deposition of Dielectrics on Graphene. *Small* **2014**, *10*, 2293−2299.

(13) Kim, K.; Zhao, Y.; Jang, H.; Lee, S.; Kim, J.; Ahn, J.; Kim, P.; Choi, J.; Hong, B. Large-Scale Pattern Growth of Graphene Films for Stretchable Transparent Electrodes. *Nature* **2009**, *457*, 706−710.

(14) Li, X.; Cai, W.; An, J.; Kim, S.; Nah, J.; Yang, D.; Piner, R.; Velamakanni, A.; Jung, I.; Tutuc, E.; Banerjee, S.; Colombo, L.; Ruoff, R. Large-Area Synthesis of High-Quality and Uniform Graphene Films on Copper Foils. *Science* **2009**, *324*, 1312−1314.

(15) Pirkle, A.; Chan, J.; Venugopal, A.; Hinojos, D.; Magnuson, C. W.; McDonnell, S.; Colombo, L.; Vogel, E. M.; Ruoff, R. S.; Wallace, R. M. The Effect of Chemical Residues on the Physical and Electrical Properties of Chemical Vapor Deposited Graphene Transferred to SiO_2. *Appl. Phys. Lett.* **2011**, *99*, 112108.

(16) Coy-Diaz, H.; Addou, R.; Batzill, M. Interface between Graphene and $SrTiO_3$(001) Investigated by Scanning Tunneling Microscopy and Photoemission. *J. Phys. Chem. C* **2013**, *117*, 21006−21013.

(17) Coy Diaz, H.; Addou, R.; Batzill, M. Interface Properties of CVD Grown Graphene Transferred onto MoS_2(0001). *Nanoscale* **2014**, *6*, 1071−1078.

(18) Dahal, A.; Addou, R.; Coy-Diaz, H.; Batzill, M. Wet-transfer of CVD-grown Graphene onto Sulfur-Protected W(110). *Surf. Sci.* **2014**, DOI: 10.1016/j.susc.2014.09.003.

(19) Wallace, R. M. In-Situ Studies of Interfacial Bonding of High-κ Dielectrics for CMOS Beyond 22nm. *ECS Trans.* **2008**, *16*, 255−271.

(20) Pirkle, A.; McDonnell, S.; Lee, B.; Kim, J.; Colombo, L.; Wallace, R. M. The Effect of Graphite Surface Condition on the Composition of Al_2O_3 by Atomic Layer Deposition. *Appl. Phys. Lett.* **2010**, *97*, 082901.

(21) Swartz, A. G.; Odenthal, P. M.; Hao, Y.; Ruoff, R. S.; Kawakami, R. K. Integration of the Ferromagnetic Insulator EuO onto Graphene. *ACS Nano* **2012**, *6*, 10063−10069.

(22) Barreca, D.; Battiston, G. A.; Berto, D.; Gerbasi, R.; Tondello, E. Y_2O_3 Thin Films Characterized by XPS. *Surf. Sci. Spectra* **2001**, *8*, 234−239.

(23) Renault, O.; Gosset, L. G.; Rouchon, D.; Ermolieff, A. Angle-resolved X-ray Photoelectron Spectroscopy of Ultrathin Al_2O_3 Films Grown by Atomic Layer Deposition. *J. Vac. Sci. Technol., A* **2002**, *20*, 1867−1876.

(24) Lee, B. K.; Park, S. Y.; Kim, H. C.; Cho, K.; Vogel, E. M.; Kim, M. J.; Wallace, R. M.; Kim, J. Y. Conformal Al_2O_3 Dielectric Layer Deposited by Atomic Layer Deposition for Graphene-Based Nanoelectronics. *Appl. Phys. Lett.* **2008**, *92*, 203102.

(25) Dahal, A.; Addou, R.; Coy-Diaz, H.; Lallo, J.; Batzill, M. Charge Doping of Graphene in Metal/Graphene/Dielectric Sandwich Strucutre Evaluated by C-1s Core Level Photoemission Spectroscopy. *APL Mater.* **2013**, *1*, 042107.

(26) Lin, W.-H.; Chen, T.-H.; Chang, J.-K.; Taur, J.-I.; Lo, Y.-Y.; Lee, W.-L.; Chang, C.-S.; Su, W.-B.; Wu, C.-I. A Direct and Polymer-Free Method for Transferring Graphene Grown by Chemical Vapor Deposition to any Substrate. *ACS Nano* **2014**, *8*, 1784−1791.

DOI: 10.1021/am508154n
ACS Appl. Mater. Interfaces 2015, 7, 2082−2087